Quasisymmetry protected Ising spin-orbit coupling

L. L. Tao,[1,*] Qin Zhang,[1] Huinan Li,[1] Xianjie Wang,[1,†] Yi Wang,[1] Yu Sui,[1] Bo Song,[2] and M. Ye. Zhuravlev[3]

[1]*School of Physics, Harbin Institute of Technology, Harbin 150001, China*

[2]*National Key Laboratory of Science and Technology on Advanced Composites in Special Environments, Harbin Institute of Technology, Harbin 150001, China*

[3]*St. Petersburg State University, St. Petersburg 190000, Russia*

(Received 18 January 2023; accepted 31 March 2023; published 10 April 2023)

Quasisymmetry is an approximated symmetry in the sense that it is not the crystalline symmetry but commutes with the Hamiltonian at a lower order. Unlike exact symmetry, quasisymmetry emerges in the context of low-energy effective theory. One of the most desirable properties added by quasisymmetry is the large Berry curvatures due to the perturbatively small band gaps, which are robust against chemical and physical perturbations. Ising spin-orbit coupling (SOC) is a special type of SOC with electron spins polarizing to out-of-plane direction and can protect the spin coherence against the relaxation. For Ising-type superconductors, Ising SOC significantly affects the superconducting properties such as Pauli limit. It is commonly believed that the out-of-plane mirror symmetry M_z is necessary for Ising SOC, which puts a constraint on the allowed materials. Here we demonstrate that the strong Ising SOC exists beyond the system with M_z symmetry and is protected by the quasisymmetry. Based on the group-theoretical analysis and density-functional theory calculations, we show that the lower-order SOC Hamiltonian for certain representation is Ising type, which is protected by the quasisymmetry. Several promising systems with strong Ising SOC of several hundreds of meV near the Fermi energy are identified. In addition, we propose the general design principles to search for the realistic materials. Our results advance the fundamental understanding of Ising spin-orbit physics and greatly broaden the range of the materials hosting the Ising SOC.

DOI: 10.1103/PhysRevB.107.155412

I. INTRODUCTION

Spin-orbit coupling (SOC) is a relativistic interaction between the spin degree of freedom and the orbital motion of electrons and plays an important role in the emergence of new physical phenomena [1], such as current-induced spin polarization [2], (quantum) spin Hall effect [3–5], spin-orbit torques [6], spin-valley locking [7–9], topological states [10,11], etc. The SOC in nonmagnetic crystals without inversion symmetry is characterized by the spin splitting of bands and specific spin texture-spin arrangement in the momentum space, which is the expectation value of the spin operator on a Bloch state. Depending on the point group (PG) symmetry, the SOC may exhibit Rashba, Dresselhaus, Weyl, Ising, or more intricate types [12–15]. For example, the Rashba SOC exists for the PGs C_{3v} [16,17], C_{4v} [18,19], D_6, and C_{6v} [20] while the PGs D_3 [21,22], D_4, T, and O [23] sustain the Weyl SOC. Such rich SOC phenomena have fundamental interest and promising applications for the spintronic devices [24,25]. For instance, Rashba SOC can be utilized to design spin transistor, generate nonequilibrium spin polarization [2,26], and engineer topological insulators and superconductors etc. [27,28]. Weyl SOC reveals a hedgehog spin texture and Berry curvature around a node, which is analogous to a magnetic monopole in momentum space [29]. In the case of balanced Rashba and Dresselhaus SOC [30–33], the unidirectional spin-orbit field results in a spatially periodic mode known as a persistent spin helix, which preserves the hidden SU(2) spin rotation symmetry and renders an ultimately infinite spin lifetime [30,31]. Ising SOC is a special type of SOC that pins electron spins to the out-of-plane direction [34,35] and can significantly affect many physical properties. For example, in Ising-type superconductors, Ising SOC plays a crucial role for the superconducting pairing symmetry, which significantly enhances the critical in-plane magnetic field known as the Pauli limit [36–39].

It is commonly held that Ising SOC requires two necessary symmetry conditions [34,35]: (i) inversion-symmetry broken lifting the Kramers' degeneracy at non-time-reversal-invariant momenta (non-TRIMs); (ii) out-of-plane mirror symmetry M_z. Under M_z symmetry operation, as depicted in Fig. 1(a), the plane-parallel spins (blue and yellow) are flipped while the spins (blue) perpendicular to M_z plane remain invariant due to the fact that the spin transforms as an axial vector. Thus, electron spins in momentum space are pinned to the out-of-plane directions. Among the 32 crystalline PGs, only PGs C_{3h} and D_{3h} satisfy the above two symmetry requirements [40] and thus sustain the Ising SOC, as confirmed in the monolayer transition-metal dichalcogenides [41] and certain compounds [42]. As depicted in Fig. 1(b), if M_z commutes with the Hamiltonian H of the system, namely, $[M_z, H] = 0$, spin σ_z is a good quantum number; as such, the spin-splitting

*lltao@hit.edu.cn

†wangxianjie@hit.edu.cn

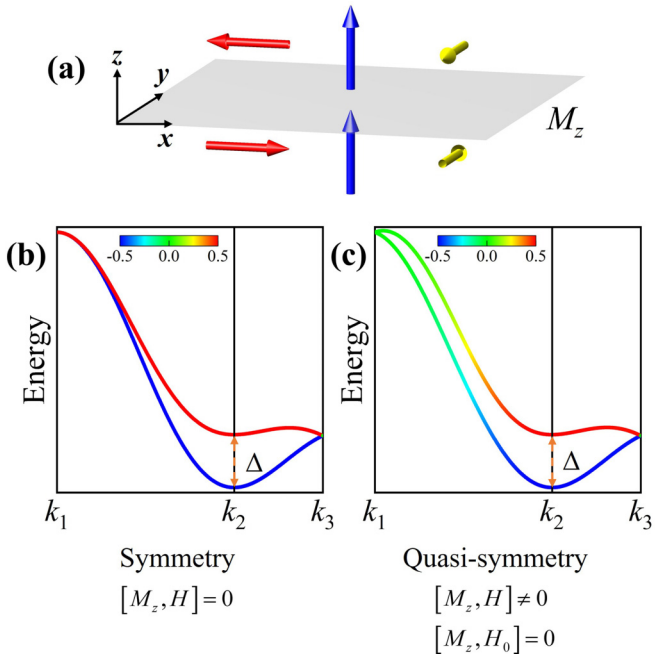

FIG. 1. (a) Sketches of mirror-symmetry M_z protected spin polarization. The spins parallel to M_z (red and yellow) change the sign while the spins perpendicular to M_z (blue) remain invariant. Sketches of spin s_z-projected band structure with SOC for the system (b) with and (c) without M_z symmetry. Δ denotes the spin splitting at k_2. $k_{1,3}$, and k_2 represent the high-symmetry TRIM and non-TRIM points, respectively. In (c), H is the total Hamiltonian while H_0 represents the lower-order expansion of H around k_2 point. The color coding quantifies s_z.

bands by SOC can be characterized by the eigenvalues ± 1 of σ_z at those non-TRIM points. It is seen that the current paradigm is based on crystalline symmetry arguments and the Ising SOC is limited to PGs C_{3h} and D_{3h}, which greatly narrows the range of realistic materials hosting Ising SOC.

In this work, we propose that Ising SOC can exist beyond the conventional PGs with M_z symmetry and is protected by the quasisymmetry [43]. Quasisymmetry is not an exact crystalline symmetry but an approximated symmetry, which commutes with the lower-order $k \cdot p$ expansion of the Hamiltonian around a high-symmetry k point [43]. Although the quasisymmetry is broken by the higher-order perturbation terms, it is sufficient to depict the essential physics and gives rise to exotic physical properties. For example, quasisymmetry in the semimetal CoSi stabilizes a near-degenerate nodal plane (below 2 meV), which results in large Berry curvatures [43,44]. Quasisymmetry protected Ising SOC can be understood from Fig. 1(c), H is the total Hamiltonian while H_0 is the lower-order expansion of H around a high-symmetry k_2 point. Although M_z is not crystalline symmetry namely $[M_z, H] \neq 0$, the first-order H_0 could commute with M_z namely $[M_z, H_0] = 0$, which protects the Ising SOC around k_2 point. As will be shown, the high-order perturbations are numerically negligible provided that the zero-order spin-splitting energy Δ is sizable. It is noteworthy that the quasisymmetry protected sizable Ising SOC is distinct from the previous demonstrated gapped node lines in the semimetal CoSi [43]. However, the essential physics for quasisymmetry protection are the same in the sense that quasisymmetry emerges in the low-energy $k \cdot p$ expansion of the Hamiltonian.

II. COMPUTATIONAL METHODS

Our density-functional theory (DFT) calculations were performed using the plane-wave ultrasoft pseudopotential method [45], as implemented in the QUANTUM ESPRESSO [46]. An energy cutoff of 544 eV for the plane-wave expansion, generalized gradient approximation (GGA) [47] for the exchange and correlation functional, and a $10 \times 10 \times 1$ k-point mesh for the self-consistent calculations were adopted throughout. The atomic coordinators were fully relaxed with the force tolerance of 2.6 meV/Å. For the SiC(0001) [Si(111)]-based surfaces, the substrate is modeled with six bilayers of 6H-SiC (Si) and the in-plane lattice constant was fixed as experimental value of 3.081 (3.840) Å. For all the surface systems, the bottom surface is saturated with hydrogen atoms and a vacuum region of 15 Å along the z direction is imposed.

III. SYMMETRY-PROTECTED ISING SOC

We begin by discussing the crystalline symmetry protected Ising SOC. As mentioned previously, only PGs C_{3h} and D_{3h} sustain the pure Ising SOC in the whole Brillouin zone (BZ) due to M_z symmetry protection. As an illustration, we consider the bulk NaSrAs, whose space group is $P\bar{6}2m$ (No. 189) and PG is D_{3h}. Figure 2(a) shows the hexagonal atomic structure with a mirror plane M_z located at Sr-As plane and the lattice constants are $a = 7.892$ Å, $c = 4.616$ Å. The corresponding first BZ is shown in Fig. 2(b). Figure 2(c) shows the band structure with SOC along the k pathes highlighted in Fig. 2(b). It is seen that bulk NaSrAs is a direct band-gap semiconductor ($\sim$0.75 eV) that the valence band maximum (VBM) and conduction-band minimum (CBM) are located at the Γ point. The color code represents the spin polarization s_z while the in-plane spin components s_x and s_y are negligible, as enforced by M_z symmetry. Since PG D_{3h} enforces SOC type $\lambda(k_y^3 - 3k_x^2 k_y)\sigma_z$ around Γ point, where λ is the SOC parameter, $k_{x,y}$ the wave numbers and σ_z the Pauli matrix. The spin texture can be calculated as $s_z = \mathrm{sgn}[\lambda \sin(3\phi)]/2$, where $\phi \equiv \tan^{-1}(k_y/k_x)$. This is exactly in accordance with the calculated spin textures around the VBM and CBM, as shown in Fig. 2(d), which reveals threefold rotation symmetry.

IV. QUASISYMMETRY PROTECTED ISING SOC

Next we move to the quasisymmetry protected Ising SOC. As an illustration, we consider the In/Si(111)-1 $\times$ 1 surface, as shown in Fig. 3(a), which is composed of monolayer In at the T_4 site of Si(111) substrate and the crystalline PG is C_{3v}. Figure 3(b) shows the band structure with SOC along the Γ-K-M line. Around K point, two distinct spin splittings can be observed: one is S1 bands with tiny spin splitting (5 meV) and the other is S2 bands with sizable spin splitting (166 meV), as seen from the three-dimensional bands (inset). Spin textures shown in Fig. 3(c)

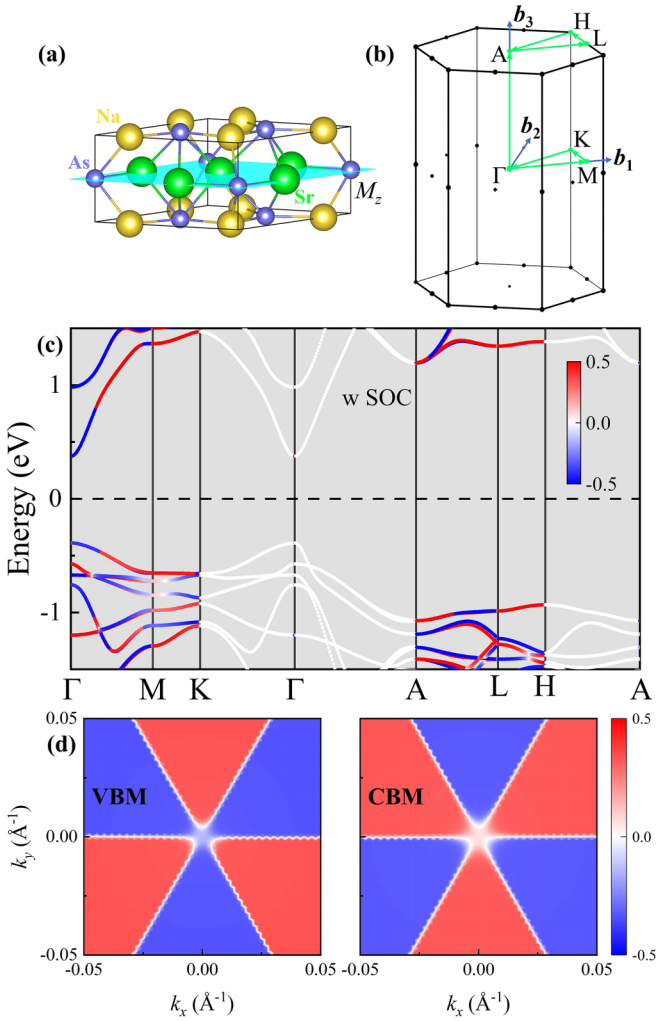

FIG. 2. (a) Crystal structure of bulk NaSrAs, the cyan colored plane denotes the mirror plane M_z. (b) The first Brillouin zone with high-symmetry k paths and k points. (c) Spin polarization s_z projected band structure with SOC. (d) Spin textures around the VBM and CBM. The color coding quantifies s_z.

exhibit an in-plane Rashba type for S1 bands and out-of-plane Ising type for S2 bands, respectively.

Such remarkably different spin splittings can be well understood from the representation-dependent atomic SOC. Especially, the PG at K is C_3, which has three one-dimensional irreducible representations A and E [40]. From the orbital-projected band structure shown in the inset of Fig. 3(b), S1 bands are composed mainly of the In-s, p_z orbitals while S2 bands are mainly formed from the In-p_x, p_y orbitals. Accordingly, S1 bands belong to the A representation while S2 bands belong to E representation without SOC and the symmetry adapted basis functions are [48]

$$|\phi_A\rangle = |p_z\rangle,\ |\phi_E^\tau\rangle = -\frac{1}{\sqrt{2}}(\tau|p_x\rangle + i|p_y\rangle), \tag{1}$$

where $\tau = \pm 1$ is the valley index and the two valleys are related by time-reversal operation. The atomic SOC is given by $\lambda \mathbf{L}\cdot\mathbf{S}$ [48,49], where $\mathbf{L}$ ($\mathbf{S}$) is the orbital (spin) angular momentum operator and λ is the intra-atomic SOC

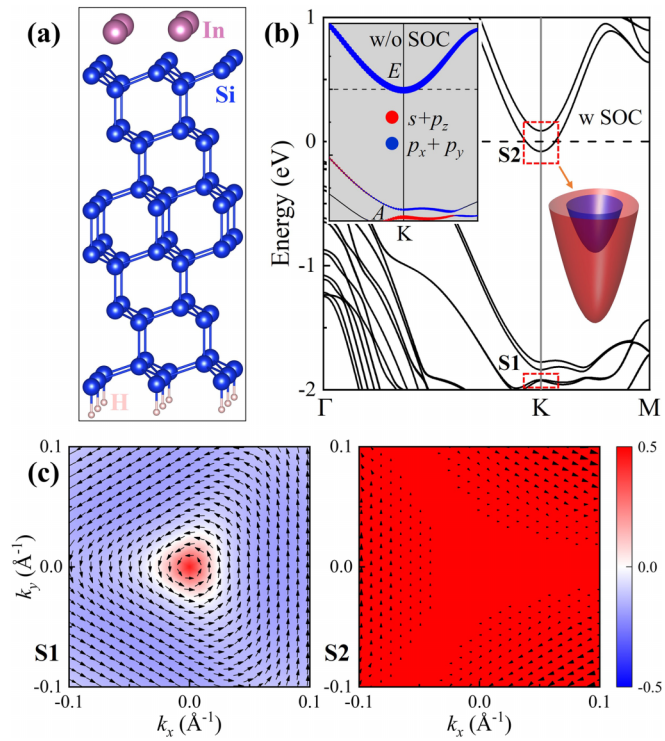

FIG. 3. (a) Atomic structure of the In/Si(111)-1 × 1 interface with the T_4 adsorption site, namely the site above the second layer atoms from the surface. (b) Band structure with SOC along the Γ-K-M line. The Fermi level is aligned to zero as indicated by the dashed lines. Inset: Orbital-projected band structure onto In-s, p orbitals around K without SOC; three-dimensional band structure of S2 bands around K. (c) Spin textures around K for the lower branch of S1 and S2 bands as highlighted by dashed boxes in (b). The in-plane spin components $s_{x,y}$ are shown by arrows while the out-of-plane spin component s_z is indicated by color.

constant. It can be calculated that $\langle\phi_A|\lambda\mathbf{L}\cdot\mathbf{S}|\phi_A\rangle = 0$ and $\langle\phi_E^\tau|\lambda\mathbf{L}\cdot\mathbf{S}|\phi_E^\tau\rangle = \lambda\tau\sigma_z$, which naturally explains the distinct spin splittings between S1 and S2 bands around K. We see that the SOC around K under lower-order approximation for S2 bands is $H_0 = \lambda\tau\sigma_z$, which is an Ising type. Since the mirror operator $M_z = i\sigma_z$ commutes with H_0 namely $[M_z, H_0] = 0$, which forbids the existence of $\sigma_{x,y}$-dependent SOC terms, Ising SOC is protected by M_z although M_z is not the crystalline symmetry of In/Si(111)-1 × 1 surface. In the spinful case, $M_z^2 = -1$ and hence bands can be characterized by the eigenvalues $\pm i$ of M_z for S2 bands around K. By using the method of invariants [12,50], the linear-order H_1 and cubic-order H_2 terms are given by

$$\begin{aligned} H_1 &= [\alpha(\cos\phi\sigma_x + \sin\phi\sigma_y) + \beta(\cos\phi\sigma_y - \sin\phi\sigma_x)]k, \\ H_2 &= [\gamma_1(\cos\phi\sigma_x + \sin\phi\sigma_y) + \gamma_2(\cos\phi\sigma_y - \sin\phi\sigma_x) \\ &\quad + \delta_1\cos(3\phi)\sigma_z + \delta_2\sin(3\phi)\sigma_z]k^3, \end{aligned} \tag{2}$$

where α, β, $\gamma_{1,2}$, and $\delta_{1,2}$ are independent SOC parameters and $\phi \equiv \tan^{-1}(k_y/k_x)$. Since $[M_z, H_{1,2}] \neq 0$, the quasisymmetry M_z is broken by $H_{1,2}$ terms and SOC is no longer the Ising type. One can evaluate the effect of higher-order perturbation terms via the degenerate perturbation theory. Specifically, the eigenvalues and eigenstates of H_0 take the

TABLE I. Spin-splitting energy Δ at K for a series of semiconductor surfaces with adsorbed heavy atoms. The definition of Δ for the corresponding surface system is given in the Supplemental Material, Fig. S1 [53]. d represents the equilibrium interlayer distances between heavy atoms and substrates. The second column represents the most stable configuration with the lowest energy.

System	Configuration	d (Å)	Δ (meV)
Ga/Si(111)	T_4	1.89	55
In/Si(111)	T_4	2.19	166
Tl/Si(111)	T_4	2.29	642
Ge/SiC(111)	T_1	2.51	119
Sn/SiC(111)	T_1	2.72	157
Pb/SiC(111)	T_1	2.81	149
Sb/Si(111)	T_4	2.05	236
Bi/Si(111)	T_4	2.28	839

form $E_s^0 = s\lambda$, $\psi_s^0 = \chi_s$, where $s = \pm 1$ is the spin index and χ_s are the eigenstates of σ_z. Up to the second-order correction, the eigenvalues E_s and eigenstates ψ_s can be calculated as

$$\begin{aligned} E_s &= \frac{\hbar^2 k^2}{2m} + s\lambda + s\frac{(\alpha^2+\beta^2)k^2 + (\gamma_1^2+\gamma_2^2)k^6}{\Delta} \\ &\quad + s[\delta_1\cos(3\phi) + \delta_2\sin(3\phi)]k^3, \\ \psi_s &= e^{i\mathbf{k}\cdot\mathbf{r}}\Big[\chi_s + s\frac{(\alpha + is\beta)ke^{is\phi}}{\Delta}\chi_{-s} \\ &\quad + s\frac{(\gamma_1 + is\gamma_2)k^3 e^{is\phi}}{\Delta}\chi_{-s}\Big], \end{aligned} \tag{3}$$

where $\Delta = 2\lambda$ denotes the zero-order spin-splitting energy. From Eq. (3), the second-order correction is inversely proportional to Δ and is thus numerically negligible as long as Δ is rather large. This is indeed the case that $\Delta = 166$ meV at K for S2 bands is sizable. Moreover, Δ around K is approximately an constant spanning a large area (0.1 Å$^{-1}\times$0.1 Å^{-1}) of BZ in the sense that the deviation is less than 5 meV, as seen from the inset of Fig. 3(b).

In addition to the above In/Si(111)-1 × 1 surface, the strong Ising SOC protected by quasisymmetry is expected to exist in other surface systems. Table I lists a series of semiconductor surfaces with adsorbed heavy atoms in the most stable configuration (second column). It is noteworthy that the surface systems Tl/Si(111) and Sn/SiC(111) have also been studied by previous work [51,52], although the point of quasisymmetry protected Ising SOC was not mentioned. Those surface systems have crystalline PG C_{3v}, for which M_z symmetry is absent. First, one can see that the interlayer distance d increases monotonically with increasing the atomic number for the same substrates and the variation of spin-splitting energy Δ shows a similar trend. Intriguingly, Δ at K (see Supplemental Material, Fig. S1 for the definition of Δ [53]) are several hundreds of meV for the adsorbed atoms with large atomic numbers. For example, Δ for the Bi/Si(111) surface is more than 800 meV, which is significantly large. As a comparison, the spin splittings of the valence bands at K for the transition-metal dichalcogenides are ranging from more than 100 meV (MoS_2) to 400 meV (WTe_2) [54].

It is instructive to compare the major differences between symmetry and quasisymmetry protected Ising SOC. For the former, the lattice distortions or imperfections such as vacancies and impurities likely break the M_z symmetry and are detrimental to Ising SOC. As distinct from proper symmetry, quasisymmetry acts selectively on the subsets of system [43] and are hence more immune to the symmetry-breaking lattice distortions. For example, quasisymmetry M_z for the In/Si(111)-1 × 1 surface only acts on the adsorbed In layer and Ising SOC is therefore insensitive to the symmetry broken of Si(111) substrate.

V. DESIGN PRINCIPLES

Having demonstrated the existence of quasisymmetry protected Ising SOC for certain surface systems, we now move to the establishment of its general design principles, which could help with the future search of realistic materials hosting Ising SOC. Based on the above discussion, we find that two prerequisite conditions are crucial for the occurrence of Ising SOC: one is heavy atoms and the other is specific representation at non-TRIM points. Indeed, as seen from Table I, heavier atoms favor the enhancement of atomic SOC, which protects the robustness of Ising SOC against the higher-order perturbation. On the other hand, certain representation vanishes the $\sigma_{x,y}$-dependent terms, which is crucial for Ising SOC. To see this, according to $k \cdot p$ perturbation theory, the general SOC Hamiltonian is given by [48]

$$H_{\mathrm{SOC}} = H_0 + H_{\mathbf{k}}, \tag{4}$$

where H_0 ($H_{\mathbf{k}}$) is the k-independent (k-dependent) SOC. As stated above, H_0 is given by $\lambda\mathbf{L}\cdot\mathbf{S}$, which can be rewritten as $\lambda/2(L_+\sigma_- + L_-\sigma_+ + 2L_z\sigma_z)$, where $L_\pm \equiv L_x \pm iL_y$ and $\sigma_\pm \equiv \sigma_x \pm i\sigma_y$ are the ladder operators. Generally, H_0 is obtained by calculating the expectation value of $\mathbf{L}\cdot\mathbf{S}$ on a given Bloch function $u_{\mathbf{k}}(\mathbf{r})$, namely $H_0 \sim \langle u_{\mathbf{k}}|\mathbf{L}\cdot\mathbf{S}|u_{\mathbf{k}}\rangle$ [48]. To satisfy Ising SOC namely $H_0 \sim \sigma_z$, it is required $\langle u_{\mathbf{k}}|\mathbf{L}\cdot\mathbf{S}|u_{\mathbf{k}}\rangle = \langle u_{\mathbf{k}}|L_z\sigma_z|u_{\mathbf{k}}\rangle$. It is known that, close to the nucleus, $|u_{\mathbf{k}}\rangle$ is well described by a linear combination of atomic orbitals [25,48]. According to representation theory of groups [40], the spherical harmonics $|lm\rangle$ are the basis functions for the certain representations of PGs. Then, we have $\langle lm|\lambda\mathbf{L}\cdot\mathbf{S}|lm\rangle = \langle lm|\lambda L_z\sigma_z|lm\rangle = \lambda m\sigma_z$. For example, within the E-representation basis functions for PG C_3 $|\phi_E\rangle = |1, \pm 1\rangle$ in Eq. (1), we have $\langle\phi_E|\lambda\mathbf{L}\cdot\mathbf{S}|\phi_E\rangle = \lambda\sigma_z$. Besides the p-orbital systems investigated in this work, the quasisymmetry protected Ising SOC is also expected in d-orbital systems. For example, using d orbitals, the E-representation basis functions can be constructed as [41]

$$\begin{aligned} |\phi_E^\tau\rangle &= \frac{1}{\sqrt{2}}(|d_{x^2-y^2}\rangle + i\tau|d_{xy}\rangle), \\ |\phi_E^\tau\rangle &= -\frac{1}{\sqrt{2}}(|d_{zx}\rangle + i\tau|d_{yz}\rangle). \end{aligned} \tag{5}$$

Within the orbital basis Eq. (5), we have $\langle\phi_E^\tau|\lambda\mathbf{L}\cdot\mathbf{S}|\phi_E^\tau\rangle = 2\lambda\tau\sigma_z$. Thus, E representation H_0 is Ising type.

VI. SUMMARY AND DISCUSSION

In summary, in the spirit of quasisymmetry, we have shown that Ising SOC exists in the system even without M_z symmetry and identified several promising surface systems, which features strong Ising SOC of several hundreds of meV near the Fermi energy. It is found that M_z operator is an exact symmetry at lower-order expansion of Hamiltonian and the higher-order correction is inversely proportional to the zero-order spin splitting. Thus, Ising SOC is robust against the higher-order perturbation provided that zero-order spin splitting is sizable. Our proposed mechanism removes the previously established constraints on the allowed materials and greatly broadens the range of materials hosting Ising SOC. Importantly, we establish the general design principles that could help with the future prediction and search of realistic materials. In addition, the present work suggests another benefit offered by quasisymmetry in addition to the large Berry curvature demonstrated previously [43], which expands the quasisymmetry physics and advances the symmetry-dictated SOC. Looking forward, the interplay between quasisymmetry and SOC may give rise to some distinct features overlooked previously. Furthermore, one could explore the new topological states such as topological superconductors and Majorana fermions by making use of the strong Ising SOC.

ACKNOWLEDGMENTS

The authors thank Qihang Liu for helpful discussions. This work is supported by the Fundamental Research Funds for the Central Universities (FRFCU5710053421) and the National Natural Science Foundation of China (Grant No. 12274102). Computations were performed at the Shanghai Supercomputer Center and the atomic structures were produced using the VESTA software [55].

[1] A. Soumyanarayanan, N. Reyren, A. Fert, and C. Panagopoulos, Emergent phenomena induced by spin-orbit coupling at surfaces and interfaces, Nature (London) **539**, 509 (2016).
[2] R. H. Silsbee, Spin-orbit induced coupling of charge current and spin polarization, J. Phys.: Condens. Matter **16**, R179 (2004).
[3] J. Sinova, S. O. Valenzuela, J. Wunderlich, C. H. Back, and T. Jungwirth, Spin Hall effects, Rev. Mod. Phys. **87**, 1213 (2015).
[4] C. L. Kane and E. J. Mele, Quantum Spin Hall Effect in Graphene, Phys. Rev. Lett. **95**, 226801 (2005).
[5] B. A. Bernevig and S. C. Zhang, Quantum Spin Hall Effect, Phys. Rev. Lett. **96**, 106802 (2006).
[6] A. Manchon, J. Železný, I. M. Miron, T. Jungwirth, J. Sinova, A. Thiaville, K. Garello, and P. Gambardella, Current-induced spin-orbit torques in ferromagnetic and antiferromagnetic systems, Rev. Mod. Phys. **91**, 035004 (2019).
[7] X. Xu, W. Yao, D. Xiao, and T. F. Heinz, Spin and pseudospins in layered transition metal dichalcogenides, Nature Phys. **10**, 343 (2014).
[8] L. L. Tao and E. Y. Tsymbal, Two-dimensional spin-valley locking spin valve, Phys. Rev. B **100**, 161110(R) (2019).
[9] L. L. Tao, A. Naeemi, and E. Y. Tsymbal, Valley-Spin Logic Gates, Phys. Rev. Appl. **13**, 054043 (2020).
[10] M. Z. Hasan and C. L. Kane, *Colloquium:* Topological insulators, Rev. Mod. Phys. **82**, 3045 (2010).
[11] X. L. Qi and S. C. Zhang, Topological insulators and superconductors, Rev. Mod. Phys. **83**, 1057 (2011).
[12] Sz. Vajna, E. Simon, A. Szilva, K. Palotas, B. Ujfalussy, and L. Szunyogh, Higher-order contributions to the Rashba-Bychkov effect with application to the Bi/Ag(111) surface alloy, Phys. Rev. B **85**, 075404 (2012).
[13] L. L. Tao and E. Y. Tsymbal, Perspectives of spin-textured ferroelectrics, J. Phys. D **54**, 113001 (2021).
[14] C. Mera Acosta, L. Yuan, G. M. Dalpian, and A. Zunger, Different shapes of spin textures as a journey through the Brillouin zone, Phys. Rev. B **104**, 104408 (2021).
[15] P. Liu, J. Li, J. Han, X. Wan, and Q. Liu, Spin-Group Symmetry in Magnetic Materials with Negligible Spin-Orbit Coupling, Phys. Rev. X **12**, 021016 (2022).
[16] K. Ishizaka, M. S. Bahramy, H. Murakawa, M. Sakano, T. Shimojima, T. Sonobe, K. Koizumi, S. Shin, H. Miyahara, A. Kimura *et al.*, Giant Rashba-type spin splitting in bulk BiTeI, Nature Mater. **10**, 521 (2011).
[17] D. Di Sante, P. Barone, R. Bertacco, and S. Picozzi, Electric control of the giant rashba effect in bulk gete, Adv. Mater. **25**, 313 (2013).
[18] L. L. Tao and J. Wang, Strain-tunable ferroelectricity and its control of Rashba effect in $KTaO_3$, J. Appl. Phys. **120**, 234101 (2016).
[19] L. G. D. da Silveira, P. Barone, and S. Picozzi, Rashba-Dresselhaus spin-splitting in the bulk ferroelectric oxide $BiAlO_3$, Phys. Rev. B **93**, 245159 (2016).
[20] A. Narayan, Class of Rashba ferroelectrics in hexagonal semiconductors, Phys. Rev. B **92**, 220101(R) (2015).
[21] M. Sakano, M. Hirayama, T. Takahashi, S. Akebi, M. Nakayama, K. Kuroda, K. Taguchi, T. Yoshikawa, K. Miyamoto, T. Okuda *et al.*, Radial Spin Texture in Elemental Tellurium with Chiral Crystal Structure, Phys. Rev. Lett. **124**, 136404 (2020).
[22] G. Gatti, D. Gosálbez-Martínez, S. S. Tsirkin, M. Fanciulli, M. Puppin, S. Polishchuk, S. Moser, L. Testa, E. Martino, S. Roth *et al.*, Radial Spin Texture of the Weyl Fermions in Chiral Tellurium, Phys. Rev. Lett. **125**, 216402 (2020).
[23] W. Tan, X. Jiang, Y. Li, X. Wu, J. Wang, and B. Huang, A unified understanding of diverse spin textures of kramers-weyl fermions in nonmagnetic chiral crystals, Adv. Funct. Mater. **32**, 2208023 (2022).
[24] A. Manchon, H. C. Koo, J. Nitta, S. M. Frolov, and R. A. Duine, New perspectives for Rashba spin-orbit coupling, Nature Mater. **14**, 871 (2015).
[25] G. Bihlmayer, P. Noel, D. V. Vyalikh, E. V. Chulkov, and A. Manchon, Rashba-like physics in condensed matter, Nature Rev. Phys. **4**, 642 (2022).
[26] L. L. Tao and E. Y. Tsymbal, Spin-orbit dependence of anisotropic current-induced spin polarization, Phys. Rev. B **104**, 085438 (2021).

[27] S. Nakosai, Y. Tanaka, and N. Nagaosa, Topological Superconductivity in Bilayer Rashba System, Phys. Rev. Lett. **108**, 147003 (2012).
[28] T. Das and A. V. Balatsky, Engineering three-dimensional topological insulators in Rashba-type spin-orbit coupled heterostructures, Nature Commun. **4**, 1972 (2013).
[29] J. H. Dil, Finding spin hedgehogs in chiral crystals, Physics **13**, 45 (2020).
[30] B. A. Bernevig, J. Orenstein, and S. C. Zhang, Exact SU(2) Symmetry and Persistent Spin Helix in a Spin-Orbit Coupled System, Phys. Rev. Lett. **97**, 236601 (2006).
[31] J. Schliemann, *Colloquium*: Persistent spin textures in semiconductor nanostructures, Rev. Mod. Phys. **89**, 011001 (2017).
[32] L. L. Tao and E. Y. Tsymbal, Persistent spin texture enforced by symmetry, Nature Commun. **9**, 2763 (2018).
[33] X.-Z. Lu and J. M. Rondinelli, Discovery principles and materials for symmetry-protected persistent spin textures with long spin lifetimes, Matter **3**, 1211 (2020).
[34] B. T. Zhou, N. F. Q. Yuan, H. L. Jiang, and K. T. Law, Ising superconductivity and Majorana fermions in transition-metal dichalcogenides, Phys. Rev. B **93**, 180501(R) (2016).
[35] C. Wang, Y. Xu, and W. Duan, Ising superconductivity and its hidden variants, Acc. Mater. Res. **2**, 526 (2021).
[36] J. M. Lu, O. Zheliuk, I. Leermakers, N. F. Q. Yuan, U. Zeitler, K. T. Law, and J. T. Ye, Evidence for two-dimensional ising superconductivity in gated MoS_2, Science **350**, 1353 (2015).
[37] X. Xi, Z. Wang, W. Zhao, J. H. Park, K. T. Law, H. Berger, L. Forro, J. Shan, and K. F. Mak, Ising pairing in superconducting $NbSe_2$ atomic layers, Nature Phys. **12**, 139 (2016).
[38] S. C. de la Barrera, Michael R. Sinko, D. P. Gopalan, N. Sivadas, K. L. Seyler, K. Watanabe, T. Taniguchi, A. W. Tsen, X. Xu, D. Xiao, and B. M. Hunt, Tuning ising superconductivity with layer and spin–orbit coupling in two-dimensional transition-metal dichalcogenides, Nature Commun. **9**, 1427 (2018).
[39] H. Yi, L. H. Hu, Y. Wang, R. Xiao, J. Cai, D. R. Hickey, C. Dong, Y. F. Zhao, L. J. Zhou, R. Zhang *et al.*, Crossover from Ising- to Rashba-type superconductivity in epitaxial Bi_2Se_3/monolayer $NbSe_2$ heterostructures, Nature Mater. **21**, 1366 (2022).
[40] M. Tinkham, *Group Theory and Quantum Mechanics* (Dover, Minola, 2003).
[41] D. Xiao, G. B. Liu, W. Feng, X. Xu, and W. Yao, Coupled Spin and Valley Physics in Monolayers of MoS_2 and Other Group-VI Dichalcogenides, Phys. Rev. Lett. **108**, 196802 (2012).
[42] H. J. Zhao, H. Nakamura, R. Arras, C. Paillard, P. Chen, J. Gosteau, X. Li, Y. Yang, and L. Bellaiche, Purely Cubic Spin Splittings with Persistent Spin Textures, Phys. Rev. Lett. **125**, 216405 (2020).
[43] C. Guo, L. Hu, C. Putzke, J. Diaz, X. Huang, K. Manna, F.-R. Fan, C. Shekhar, Y. Sun, C. Felser, C. Liu, B. A. Bernevig, and P. J. W. Moll, Quasi-symmetry-protected topology in a semi-metal, Nature Phys. **18**, 813 (2022).
[44] M. A. Wilde and C. Pfleiderer, Large curvature near a small gap, Nature Phys. **18**, 731 (2022)
[45] D. Vanderbilt, Soft self-consistent pseudopotentials in a generalized eigenvalue formalism, Phys. Rev. B **41**, 7892(R) (1990).
[46] P. Giannozzi, S. Baroni, N. Bonini, M. Calandra, R. Car, C. Cavazzoni, D. Ceresoli, G. L. Chiarotti, M. Cococcioni, I. Dabo *et al.*, QUANTUM ESPRESSO: a modular and open-source software project for quantum simulations of materials, J. Phys.: Condens. Matter **21**, 395502 (2009).
[47] J. P. Perdew, K. Burke, and M. Ernzerhof, Generalized Gradient Approximation Made Simple, Phys. Rev. Lett. **77**, 3865 (1996).
[48] R. Winkler, *Spin-Orbit Coupling Effects in Two-Dimensional Electron and Hole Systems*, Springer Tracts in Modern Physics (Springer, Berlin, 2003).
[49] J. Li, Q. Yao, L. Wu, Z. Hu, B. Gao, X. Wan, and Q. Liu, Designing light-element materials with large effective spin-orbit coupling, Nature Commun. **13**, 919 (2022).
[50] G. L. Bir and G. E. Pikus, *Symmetry and Strain-Induced Effects in Semiconductors* (Wiley, New York, 1974).
[51] K. Sakamoto, T. Oda, A. Kimura, K. Miyamoto, M. Tsujikawa, A. Imai, N. Ueno, H. Namatame, M. Taniguchi, P. E. J. Eriksson, and R. I. G. Uhrberg, Abrupt Rotation of the Rashba Spin to the Direction Perpendicular to the Surface, Phys. Rev. Lett. **102**, 096805 (2009).
[52] K. Yaji, A. Visikovskiy, T. Iimori, K. Kuroda, S. Hayashi, T. Kajiwara, S. Tanaka, F. Komori, and S. Shin, Coexistence of Two Types of Spin Splitting Originating from Different Symmetries, Phys. Rev. Lett. **122**, 126403 (2019).
[53] See Supplemental Material at http://link.aps.org/supplemental/10.1103/PhysRevB.107.155412 for the band structures with SOC of the surface systems listed in Table I.
[54] G. B. Liu, W. Y. Shan, Y. Yao, W. Yao, and D. Xiao, Three-band tight-binding model for monolayers of group-VIB transition metal dichalcogenides, Phys. Rev. B **88**, 085433 (2013).
[55] K. Momma and F. Izumi, VESTA 3 for three-dimensional visualization of crystal, volumetric and morphology data, J. Appl. Crystallogr. **44**, 1272 (2011).